# Investigating Thermal Transport across the AlN/Diamond Interface via the Machine Learning Potential

Zhanpeng Sun [1, 2, #], Xiang Sun [1, 2, #], Zijun Qi [1, 2], Qijun Wang [1, 2], Rui Li [1, 2], Lijie Li [5], Gai Wu [1, 2, 3, *], Wei Shen [1, 2, 3, *], Sheng Liu [1, 2, 4]

[1] The Institute of Technological Sciences, Wuhan University, Wuhan 430072, China

[2] School of Power and Mechanical Engineering, Wuhan University, Wuhan 430072, China

[3] Hubei Key Laboratory of Electronic Manufacturing and Packaging Integration, Wuhan University, Wuhan 430072, China

[4] School of Mechanical Science and Engineering, Huazhong University of Science and Technology, Wuhan 430074, China

[5] College of Engineering, Swansea University, Swansea SA1 8EN, UK

[*] Corresponding Authors:

Gai Wu, E-mail: wugai1988@whu.edu.cn

Wei Shen, E-mail: wei_shen_@whu.edu.cn

[#] Zhanpeng Sun and Xiang Sun contributed equally to this work.

## ABSTRACT

Aluminum nitride (AlN) is an ultrawide-bandgap semiconductor with excellent potential for high-power applications. However, the heat dissipation issue remains a huge challenge for the use of AlN in high-power devices. A promising solution for this problem is to integrate AlN with the diamond heat sink. Therefore, interfacial thermal transport has become a significant bottleneck in thermal management. In this work, one neuroevolution potential is developed based on neural networks, which significantly improves the accuracy of predicting thermal properties compared to traditional potentials and address the issue of inaccurate thermal performance prediction of AlN/diamond heterostructures using traditional potentials. Molecular dynamics simulations based on NEP is adopted to investigate the crystal-orientation-dependent and interfacial-atom-dependent thermal boundary resistance of the AlN/diamond heterostructures after the interfacial bonding.

Compared to bonding with Al and C atoms, the TBR decreases by approximately 50% after bonding with N and C atoms at the interface. Especially for the AlN (0001)-N-diamond (100) heterostructure, the TBR is 0.95 $m^2 \cdot K \cdot GW^{-1}$, very close to the theoretical limit of 0.8 $m^2 \cdot K \cdot GW^{-1}$ through the diffuse mismatch model (DMM) theory. Finally, the insightful optimization strategies are proposed in this work which could pave the way for better thermal design and management of AlN/diamond heterostructures.

***Keywords:*** Thermal boundary resistance, AlN/diamond interface, Molecular dynamics, Neuroevolution potential

## 1. Introduction

Recently, Aluminum nitride (AlN) has received widespread attention due to its excellent mechanical and electrical properties [1-3]. Due to its outstanding properties such as high breakdown voltage, high electron mobility, stable high-temperature performance and good UV transmittance, AlN has been widely employed in high-power devices in communications, medical, industrial manufacturing and other fields [4]. However, the heat dissipation issue remains a huge challenge for the application of AlN in high-power devices [5]. An excellent solution is the integration of the high thermal conductivity materials with AlN to enhance the heat dissipation [6-9]. Diamond is recognized as a promising candidate for heat sinks due to its high thermal conductivity (over 2000 $W \cdot m^{-1} \cdot K^{-1}$) [10-13]. In addition, the lattice match between AlN and diamond is excellent, and the lower limit of thermal boundary resistance (TBR) for the AlN/diamond interface predicted by the diffuse mismatch model (DMM) theory is 0.8 $m^2 \cdot K \cdot GW^{-1}$ [14]. Therefore, AlN and diamond are widely regarded as promising partners.

Molecular dynamics (MD) simulations have been extensively employed to investigate the interfacial thermal transport properties of heterostructures [15-17]. However, MD simulations rely heavily on the accuracy of the interatomic potential [18]. Heterostructures are typically intricate structures composed of multiple elements, thus making it difficult for traditional potentials to provide an accurate description. This discrepancy may lead to inaccuracies in the evaluation of the TBR of heterostructures using MD methods. For instance, in a prior study, the TBR of AlN/diamond was assessed using MD methods with the Tersoff potential. Despite significant enhancements in interfacial heat transfer achieved through interface engineering, the evaluated TBR still exceeded the theoretical limit by 2 to 3 times [5].

Recent research has utilized machine learning (ML) for studying thermal transport [19-21]. In this method,

the *ab initio* potential energy surface is reconstructed using ML to achieve precise interatomic potential descriptions. Employing ML potential, other researchers have recently explored the thermal properties of graphene/borophene [22], Ge/GaAs [23], GaN/BAs [24] and so on. Compared with other ML algorithms, the neuroevolution potential (NEP) acquired via Graphics Processing Units Molecular Dynamics code (GPUMD) demonstrates superior accuracy and cost-effectiveness in atomistic simulations and heat transport applications [25-28].

In this work, the TBR of the AlN/diamond interfaces was investigated via ML potential. NEP trained specifically for AlN/diamond heterostructures were validated to exhibit improved accuracy compared to traditional potential. Concurrently, the influence of diamond crystal orientations and AlN atomic type at interfaces on TBR was also investigated. Furthermore, a more accurate potential was provided for MD simulations of heat transport in AlN/diamond heterostructures. Guided by the crystal orientations of diamond and the atomic types of AlN at the interface, insightful optimization strategies were proposed, paving the way for better thermal design and management of AlN/diamond heterostructures.

## 2. Computational methods and models

### 2.1 NEP method

The NEP model, a machine learning potential (MLP), utilizes a single neural network and is trained through a separable natural evolution strategy [29]. The NEP model generates the potential energy surface function *Ui* for atom *i* by constructing the descriptor vector $q_v^i$ ,which can be computed using the following formula [28, 30, 31]:

$$U_i = \sum_{\mu=1}^{N_{neu}} \omega_\mu^{(1)} \, tanh\left(\sum_{v=1}^{N_{des}} \omega_{\mu v}^{(0)} q_v^i - b_\mu^{(0)}\right) - b^{(1)} \quad (1)$$

where $N_{des}$ represents the number of components in the descriptor vector, $N_{neu}$ denotes the number of neurons, $tanh(x)$ stands for the activation function of the hidden layer, $\omega^{(0)}$ represents the weight matrix connecting the input layer to the hidden layer, $\omega^{(1)}$ represents the weight vector connecting the hidden layer to the output layer node $U_i$, $b^{(0)}$ is the bias vector of the hidden layer, and $b^{(1)}$ is the bias of the output layer node $U_i$. As illustrated in Fig. 1 (a), the NEP model comprises three layers: input, hidden, and output layers. In this study, the hidden layer consists of 60 neurons.

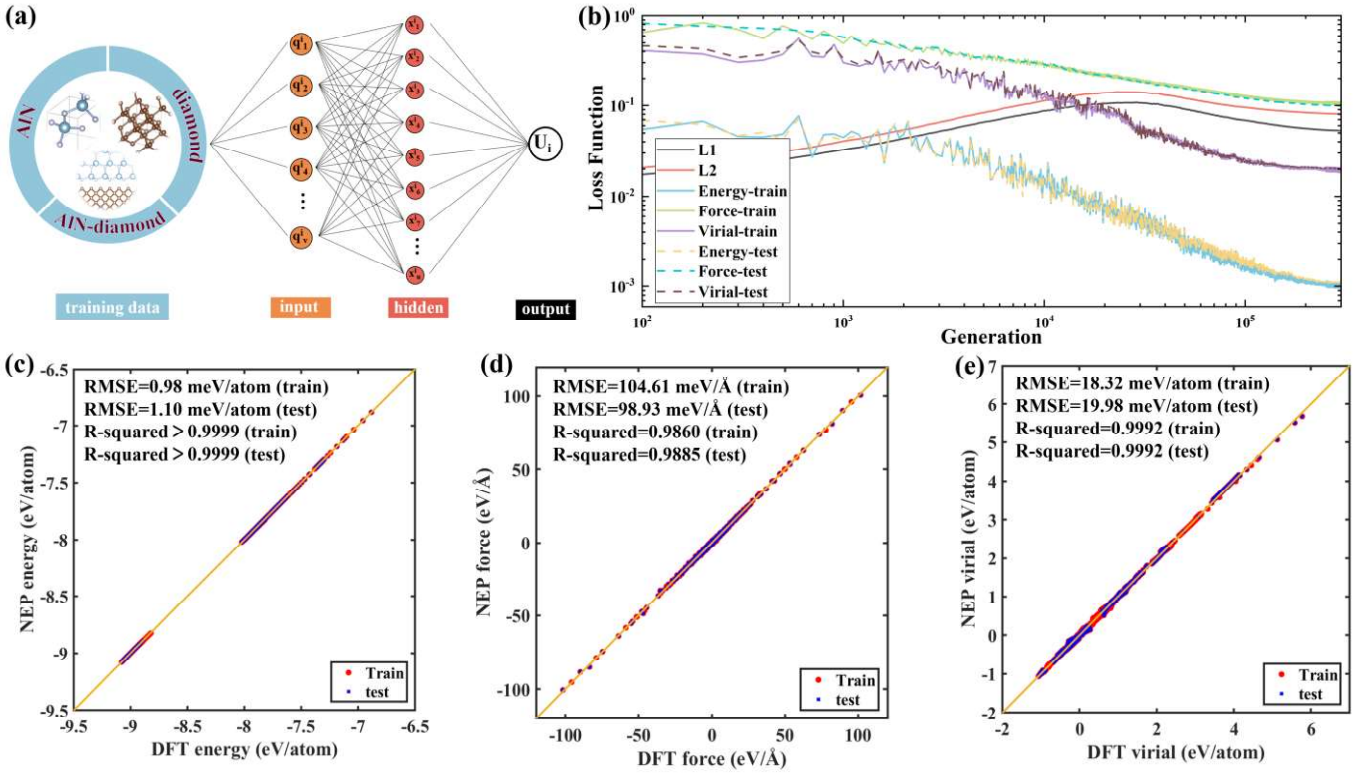


**Fig. 1.** (a) Simplified schematic representation of the NEP framework. (b) Evolution of loss functions during the training process. L1 and L2 are regularizations. (c)–(e) Comparison between the NEP predictions and DFT reference values of energy, force, and virial for the training and test sets.

## 2.2 Details of training data and mechanical behavior

For exploring heat transfer at the AlN/diamond interface, a training dataset has been built, comprising AlN, diamond, and their heterostructures. In order to be more consistent with the situation in the experiment, primary consideration is given to the (0001) planes of AlN and the (100), (110), and (111) planes of diamond. Simultaneously, the Al-C and N-C bonding at the interface of AlN/diamond including the reconstructed (100) surface of diamond have also been taken into account. Therefore, there are 6 types of heterostructures in the training set. The MD trajectories have been obtained through *ab initio* MD simulations using the Vienna *Ab Initio* Simulation Package (VASP) [32, 33], and the creation of the heterostructures in this work has mainly been conducted based on the VASPKIT [34]. Finally, *ab initio* configurations of 600 pristine AlN, 600 pristine diamond, and 2600 heterostructures have been obtained, among which 2500 configurations are included in the training dataset and 1300 configurations are included in the test dataset.

The loss terms for energy, force, and virial relations in the test and training datasets show very good convergence after 300000 generations as depicted in Fig. 1 (b). Figure 1 (c-e) display parity plots illustrating the correlations between the energies, atomic forces, and atomic virial relations predicted by the NEP and DFT, indicating strong agreement. The root-mean-squared error (RMSE) and R-squared values for the predictions

are provided as well. Typically, the RMSE values of each trained MLP model fall in the range of several meV/atom in terms of energy and several hundred meV/Å in terms of force, and all of the R-squared values for the training and test dataset are as high as more than 0.985, both indicating satisfactory training [35]. Table 1 illustrates the training hyperparameters.

**Table 1**. NEP training hyperparameters.

| Parameter | Value | Parameter | Value |
|---|---|---|---|
| $r_C^R$ | 8 Å | $r_C^A$ | 5 Å |
| $n_{max}^R$ | 12 | $n_{max}^A$ | 8 |
| $N_{basis}^R$ | 8 | $N_{basis}^A$ | 8 |
| $l_{max}^{3b}$ | 4 | $l_{max}^{4b}$ | 2 |
| $l_{max}^{5b}$ | 0 | $\lambda_1$ | 0.05 |
| $\lambda_2$ | 0.05 | $\lambda_e$ | 1.0 |
| $\lambda_f$ | 1.0 | $\lambda_v$ | 0.1 |
| $N_{neuron}$ | 60 | $N_{batch}$ | 1050 |
| $N_{population}$ | 50 | $N_{generation}$ | 300000 |

## 2.3 Equilibrium molecular dynamics (EMD) method and models

EMD simulations are employed to evaluate the thermal conductivity, based on the Green-Kubo approach [36-38]. The Green-Kubo formula connects fluctuations in heat current to thermal conductivity through the use of the autocorrelation function, as follows [39]:

$$k_\alpha(t) = \frac{1}{k_B T^2 V}\int_0^{t_0} < J_\alpha(0) J_\alpha(t) > dt \tag{2}$$

where $k_\alpha$ signifies the thermal conductivity in the α direction, $k_B$ denotes the Boltzmann constant, $V$ represents the volume of the model cell, $T$ stands for the temperature, $t_0$ indicates the integral upper limit, $J_\alpha$ denotes the component of heat current $J$ in the α direction, and $< J_\alpha(0) J_\alpha(t) >$ represents the ensemble average.

AlN has a *P63mc* crystal symmetry, and each conventional unit cell includes 2 aluminum atoms and 2 nitrogen atoms. Diamond has an *Fd-3m* crystal symmetry, and each conventional unit cell contains 8 carbon atoms. In EMD simulation, the bulk of the AlN system, consisting of $16 \times 9\sqrt{3} \times 9$ conventional unit cells, includes 10368 atoms, and the bulk of the diamond system, consisting of 10 × 10 × 10 conventional unit cells, includes 8000 atoms. Convergence tests on the model sizes have been conducted, as shown in Fig. 2. In order to exclude the size effect, the thermal conductivity at different atomic scales at 300 K has been calculated, such as the diamond with 4096, 5832 and 8000 atoms and the AlN with 6656, 8424 and 10368 atoms. It can be found that the differences in thermal conductivities among diamond and AlN structures for different cell sizes are within 5%. Thus, it can be further considered that the size effect of the thermal conductivity

calculations for diamond and AlN structures in this work can be ignored. In this work, cell structures have been visualized using VESTA software [40]. Periodic boundary conditions have been applied in all three directions. To reduce calculation errors, 50 independent MD runs have been performed to obtain the average κ values with time steps of 1 fs at 300 K.

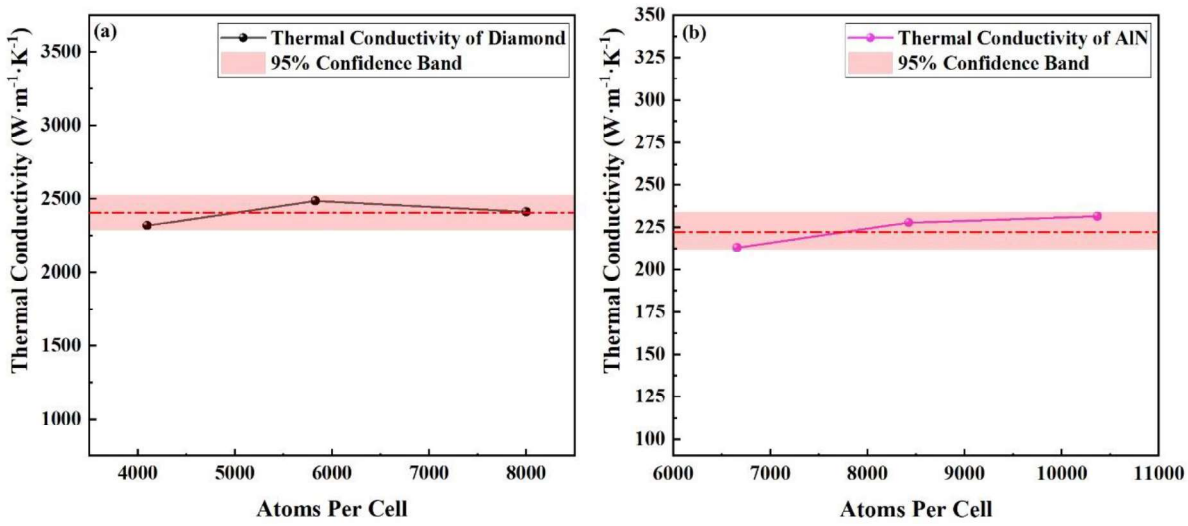


**Fig. 2.** The thermal conductivities of (a) diamond and (b) AlN with the increase of the cell size

## 2.4 Non-equilibrium molecular dynamics (NEMD) method and models

The Non-equilibrium Molecular Dynamics (NEMD) method, based on Fourier's law, divides the system into three distinct regions: a heat source continually supplying energy, a heat sink continuously releasing energy, and a measurement component for evaluating thermal conductivity. Strict adherence to the principle of energy conservation is essential in NEMD simulations. If the interatomic potential lacks sufficient accuracy, it will be very challenging to maintain a consistent energy flow from the heat source to the heat sink, the system will also collapse during the NEMD simulation [41]. Thus, NEMD simulations serve as a measure of stability for NEP. Fig. 3(b) indicates that the energy values of the heat source entering the system and the heat sink leaving the system are distributed symmetrically around E = 0, satisfying the law of energy conservation. This symmetry also confirms the sufficient accuracy of our NEP. The heat flux $J_Q$ generated in the NEMD process can be defined as:

$$J_Q = \frac{|dQ/dt|}{A} \tag{3}$$

where $|dQ/dt|$ and $A$ signify the energy exchange rate and the area of the simulation box perpendicular to the heat fluent, respectively. In order to mitigate the influence of interface area variation, the interface area of the model is set to a uniform size. The temperature difference ΔT is obtained from the temperature distribution in the abovementioned interface region. The thermal boundary resistance (TBR) can be considered analogous

to the thermal conductivity and be calculated as the formula [14]:

$$\mathrm{TBR} = \frac{\Delta \mathrm{T}}{J_Q} \tag{4}$$

A time step of 0.5 fs has been employed. Initially, a 0.1 ns heat bath has been utilized to stabilize the system temperature at 300 K, followed by a 0.5 ns equilibration period to stabilize the heat flow using the Langevin thermostat. Subsequently, the temperature profile has been acquired by running the system for 2 ns. The pertinent data are sampled every 1000 time steps and averaged every 50 data points before recording. This process has been iterated 80 times, and the ultimate temperature profile has been derived through averaging. Considering the real-world industrial scenarios, a heat source ($T_{source}$ = 325 K) and a heat sink ($T_{sink}$ = 275 K) are positioned at the ends of AlN and diamond, respectively. The heat flux proceeds from AlN to diamond. Throughout the simulation, the outermost layers in the *z* direction on both sides have been kept fixed to ensure contact with each other. Periodic boundary conditions have been applied in the *x* and *y* directions. The model size surpasses 5 × 5 × 30 nm³, encompassing over 100000 atoms (with slight variations depending on crystal orientation), as depicted in Fig. 3 (a). In heterogeneous structures composed of different crystal orientations, the mismatch between AlN and diamond in the *x*-*y* plane are all less than 1%.

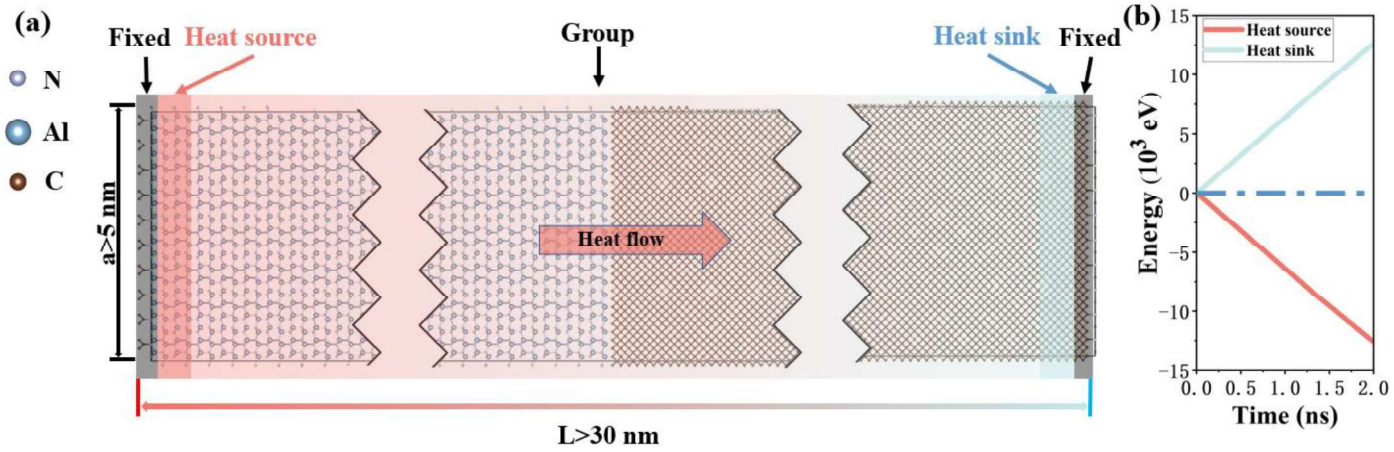


**Fig. 3.** (a) Schematic diagram of NEMD simulation. (b) The cumulative energy of the heat source domain and heat sink domain varying as a function of the simulation time.

## 3. Results and discussion

### 3.1 Bulk thermal properties

Phonon dispersion is regarded as one of the most important thermal properties, which is also commonly used for evaluating the interatomic potentials. As depicted in Fig. 4 (a, b), the phonon dispersion of AlN and

diamond calculated by NEP exhibits strong agreement with the results calculated by DFT (density functional theory) method. It is demonstrated that NEP can relatively accurately predict the thermal properties of AlN and diamond. The thermal conductivity values of diamond and AlN predicted by NEP at 300 K are shown in Fig. 4 (c). From Fig. 4 (d, e), it can be observed that while the thermal conductivity values of AlN and diamond predicted by NEP are lower than those predicted by DFT, they both exhibit better performance compared to the predictions by Tersoff. The predicted thermal conductivity based on DFT serves as the standard level, the increase predicted by NEP is 4.33% for AlN and 40.65% for diamond compared to the predictions by Tersoff. Furthermore, the thermal conductivity values predicted by NEP demonstrate excellent agreement with the reported experimental results [11, 42]. In conclusion, the NEP trained through ML will have a better performance than the traditional Tersoff potential in predicting the interfacial heat transfer in AlN/diamond heterostructures.

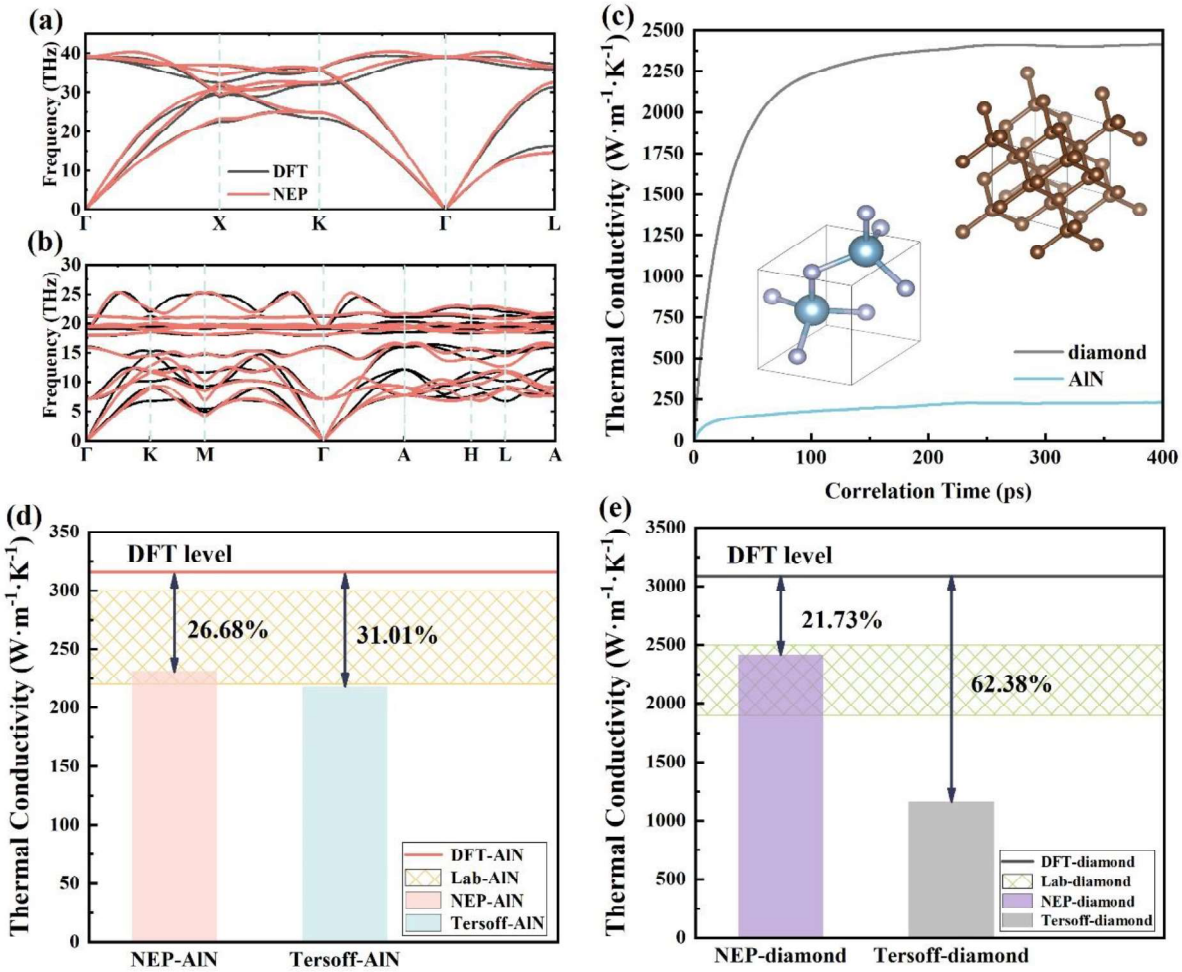


**Fig. 4.** Phonon dispersion of (a) diamond, (b) AlN. (c) Thermal conductivity of diamond and AlN at 300 K as a function of correlation time using the Green–Kubo method with the NEP, each of which is the average of 50 independent simulations. (d) A comparison between the thermal conductivity values of AlN predicted by NEP, Tersoff [5], DFT [43, 44], and experimental measurements [42]. (e) A comparison between the thermal conductivity values of diamond predicted by NEP, Tersoff [5], DFT [12], and experimental measurements [11].

## 3.2 Heat transfer in AlN/diamond interfaces

Further investigation into the interfacial heat transfer in AlN/diamond heterostructures is conducted through NEMD simulations using NEP. The stable temperature distributions of AlN/diamond heterostructures, which consist of various interfaces between AlN and diamond, are displayed in Fig. 5 (a–f). An evident temperature jump (ΔT) is observed at the AlN/diamond interface, implying the presence of a finite TBR between AlN and diamond. The TBR of the AlN (0001)-Al-diamond (100/110/111) heterostructures by interfacial bonding are all approximately 1.8 $m^2 \cdot K \cdot GW^{-1}$. Compared to previous studies using traditional potentials, the TBR increases by approximately 17%, mainly attributed to NEP's more accurate prediction of the thermal properties of AlN and diamond [5]. The TBR of the AlN (0001)-N-diamond (100/110/111) heterostructures by interfacial bonding are all approximately 1.0 $m^2 \cdot K \cdot GW^{-1}$. Especially for the AlN (0001)-N-diamond (100) heterostructure, the TBR is 0.95 $m^2 \cdot K \cdot GW^{-1}$, very close to the theoretical limit of 0.8 $m^2 \cdot K \cdot GW^{-1}$. We can observe that the crystal orientation of diamond has a relatively minor impact on TBR, whereas the bond atom types of AlN at the interface has a significant influence on TBR. The TBR of N-C bonding is nearly 50% lower than that of Al-C bonding. To further explore the reasons behind this phenomenon, the vibrational density of states (VDOS) is calculated, as shown in Fig. 6. The overlap of VDOS between N atoms and C atoms is higher compared to Al atoms and C atoms. In the AlN/diamond heterostructure, heat transfer primarily relies on lattice vibrations. The higher overlap of VDOS between N and C atoms indicates that the vibrational frequencies of N and C atoms are closer, leading to a more effective lattice vibration transmission. It is indicated to be the key reason for the lower TBR of N-C bonding compared to Al-C bonding at the interface in the AlN/diamond heterostructures.

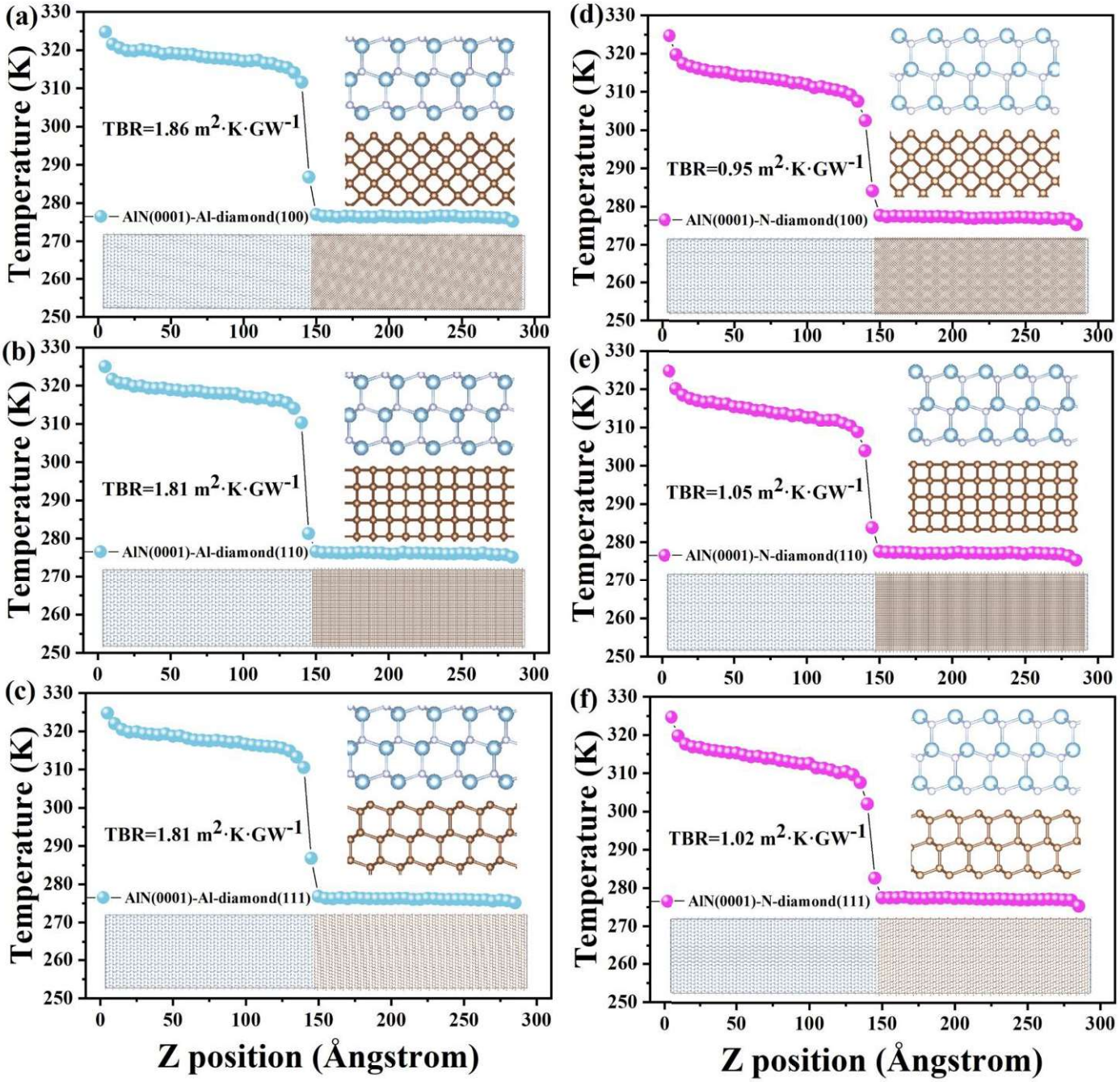


**Fig. 5.** Corresponding temperature profiles of (a) AlN (0001)-Al-diamond (100), (b) AlN (0001)-Al-diamond (110), (c) AlN (0001)-Al-diamond (111), (d) AlN (0001)-N-diamond (100), (e) AlN (0001)-N-diamond (110), and (f) AlN (0001)-N-diamond (111). The bonding at the interface in the figure is in the state before relaxation. Only the structure of the initial state is shown.

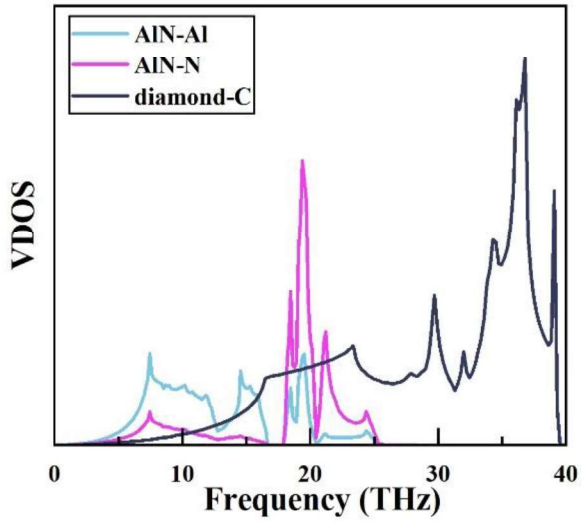


**Fig. 6.** The vibration density of states (VDOS) of AlN-Al/N and diamond-C.

## 4. Conclusion

In summary, an NEP has been trained using GPUMD to predict the thermal transfer properties at the AlN/diamond interface, based on machine learning method. The NEP has been used to predict the phonon dispersions of diamond and AlN, as well as the thermal conductivity at 300 K. The phonon dispersions predicted by NEP are in excellent agreement with the results predicted by DFT. Moreover, the thermal conductivity predicted by NEP at 300 K is in excellent agreement with previously reported experimental measurements. Although the thermal conductivity values predicted by NEP may not reach the level of DFT predictions, there is still a significant improvement compared to traditional potential.

On this basis, the TBR of the six interfaces in the AlN/diamond heterostructures have been predicted. The TBR of the AlN (0001)-Al-diamond (100/110/111) heterostructures by interfacial bonding are all approximately 1.8 $m^2 \cdot K \cdot GW^{-1}$. Compared to previous studies using traditional potentials, the TBR increases by approximately 17%. The TBR of the AlN (0001)-N-diamond (100/110/111) heterostructures by interfacial bonding are all approximately 1.0 $m^2 \cdot K \cdot GW^{-1}$. Especially for the AlN (0001)-N-diamond (100) heterostructure, the TBR is 0.95 $m^2 \cdot K \cdot GW^{-1}$, very close to the theoretical limit of 0.8 $m^2 \cdot K \cdot GW^{-1}$. It can be observed that the crystal orientation of diamond has a minimal effect on TBR, while the atomic types of AlN at the interface has a significant impact on TBR. The TBR of N-C bonding at initial interface is nearly 50% lower than that of Al-C bonding. The VDOS has been calculated to elucidate the mechanism behind this phenomenon. The main reason is that the overlap of VDOS between N and C atoms is higher compared to that between Al and C atoms. Therefore, when the interface is bonded by N atoms and C atoms, heat transfer is more efficient, resulting in a lower TBR.

## Declaration of Competing Interest

The authors declare no conflict of interest.

## Data Availability

The data that support the findings of this study are available from the corresponding author upon reasonable request. The potential file has been uploaded to the GitHub repository and is publicly available at https://github.com/doulala333/NEP-AlN-diamond.

## Acknowledgements

This work was funded by the National Natural Science Foundation of China (Grant Nos. 62004141, 52202045), the Knowledge Innovation Program of Wuhan-Shuguang (Grant Nos. 2023010201020243, 2023010201020255), the Fundamental Research Funds for the Central Universities (Grant Nos. 2042023kf0112, 2042022kf1028), the Major Program (JD) of Hubei Province (Grant No. 2023BAA009), the Hubei Natural Science Foundation (Grant No. 2022CFB606), the Open Fund of Hubei Key Laboratory of Electronic Manufacturing and Packaging Integration (Grant Nos. EMPI2024014, EMPI2024021, EMPI2023027), and the China Scholarship Council (Grant No. 202206275005).

## References

[1] O. Ambacher, Growth and applications of group III-nitrides, Journal of Physics D: Applied Physics, 31 (1998) 2653.
[2] S. Strite, H. Morkoç, GaN, AlN, and InN: a review, Journal of Vacuum Science & Technology B: Microelectronics and Nanometer Structures Processing, Measurement, and Phenomena, 10 (1992) 1237-1266.
[3] J.-M. Zhang, J. Zhang, K.-W. Xu, V. Ji, Structural, electronic and magnetic properties of the Si chains doped zigzag AlN nanoribbons, Physica E: Low-Dimensional Systems and Nanostructures, 65 (2015) 114-119.
[4] R. Yu, G. Liu, G. Wang, C. Chen, M. Xu, H. Zhou, T. Wang, J. Yu, G. Zhao, L. Zhang, Ultrawide-bandgap semiconductor AlN crystals: growth and applications, Journal of Materials Chemistry C, 9 (2021) 1852-1873.
[5] Z. Qi, W. Shen, R. Li, X. Sun, L. Li, Q. Wang, G. Wu, K. Liang, AlN/diamond interface nanoengineering for reducing thermal boundary resistance by molecular dynamics simulations, Applied Surface Science, 615 (2023) 156419.
[6] J.S. Kang, M. Li, H. Wu, H. Nguyen, T. Aoki, Y. Hu, Integration of boron arsenide cooling substrates into gallium nitride devices, Nature Electronics, 4 (2021) 416-423.

[7] Y. Cui, M. Li, Y. Hu, Emerging interface materials for electronics thermal management: experiments, modeling, and new opportunities, Journal of Materials Chemistry C, 8 (2020) 10568-10586.
[8] Y. Cui, Z. Qin, H. Wu, M. Li, Y. Hu, Flexible thermal interface based on self-assembled boron arsenide for high-performance thermal management, Nature Communications, 12 (2021) 1284.
[9] J.S. Kang, H. Wu, Y. Hu, Thermal properties and phonon spectral characterization of synthetic boron phosphide for high thermal conductivity applications, Nano Letters, 17 (2017) 7507-7514.
[10] J. Xiong, Z. Qi, K. Liang, X. Sun, Z. Sun, Q. Wang, L. Chen, G. Wu, W. Shen, Molecular dynamics insights on thermal conductivities of cubic diamond, lonsdaleite and nanotwinned diamond via the machine learned potential, Chinese Physics B, 32 (2023) 680-687.
[11] D. Onn, A. Witek, Y. Qiu, T. Anthony, W. Banholzer, Some aspects of the thermal conductivity of isotopically enriched diamond single crystals, Physical Review Letters, 68 (1992) 2806.
[12] A. Ward, D. Broido, D.A. Stewart, G. Deinzer, Ab initio theory of the lattice thermal conductivity in diamond, Physical Review B, 80 (2009) 125203.
[13] S. Li, Q. Zheng, Y. Lv, X. Liu, X. Wang, P.Y. Huang, D.G. Cahill, B. Lv, High thermal conductivity in cubic boron arsenide crystals, Science, 361 (2018) 579-581.
[14] E.T. Swartz, R.O. Pohl, Thermal boundary resistance, Reviews of Modern Physics, 61 (1989) 605.
[15] K. Ren, X. Liu, S. Chen, Y. Cheng, W. Tang, G. Zhang, Remarkable reduction of interfacial thermal resistance in nanophononic heterostructures, Advanced Functional Materials, 30 (2020) 2004003.
[16] M. Hu, X. Zhang, D. Poulikakos, C.P. Grigoropoulos, Large “near junction” thermal resistance reduction in electronics by interface nanoengineering, International Journal of Heat and Mass Transfer, 54 (2011) 5183-5191.
[17] A. Petkov, A. Mishra, J.W. Pomeroy, M. Kuball, Molecular dynamics study of thermal transport across $Ga_2O_3$–diamond interfaces, Applied Physics Letters, 122 (2023) 031602.
[18] R. Li, Z. Liu, A. Rohskopf, K. Gordiz, A. Henry, E. Lee, T. Luo, A deep neural network interatomic potential for studying thermal conductivity of β-$Ga_2O_3$, Applied Physics Letters, 117 (2020) 152102.
[19] X. Wan, W. Feng, Y. Wang, H. Wang, X. Zhang, C. Deng, N. Yang, Materials discovery and properties prediction in thermal transport via materials informatics: a mini review, Nano Letters, 19 (2019) 3387-3395.
[20] Y.-J. Wu, L. Fang, Y. Xu, Predicting interfacial thermal resistance by machine learning, npj Computational Materials, 5 (2019) 56.
[21] Z. Sun, Z. Qi, K. Liang, X. Sun, Z. Zhang, L. Li, Q. Wang, G. Zhang, G. Wu, W. Shen, A neuroevolution potential for predicting the thermal conductivity of α, β, and ε-$Ga_2O_3$, Applied Physics Letters, 123 (2023) 192202.
[22] B. Mortazavi, E.V. Podryabinkin, S. Roche, T. Rabczuk, X. Zhuang, A.V. Shapeev, Machine-learning interatomic potentials enable first-principles multiscale modeling of lattice thermal conductivity in graphene/borophene heterostructures, Materials Horizons, 7 (2020) 2359-2367.
[23] S. Wyant, A. Rohskopf, A. Henry, Machine learned interatomic potentials for modeling interfacial heat transport in Ge/GaAs, Computational Materials Science, 200 (2021) 110836.
[24] J. Wu, E. Zhou, A. Huang, H. Zhang, M. Hu, G. Qin, Deep-potential enabled multiscale simulation of gallium nitride devices on boron arsenide cooling substrates, Nature Communications, 15 (2024) 2540.
[25] Z. Fan, T. Siro, A. Harju, Accelerated molecular dynamics force evaluation on graphics processing units for thermal conductivity calculations, Computer Physics Communications, 184 (2013) 1414-1425.
[26] B. Mortazavi, Z. Fan, L.F.C. Pereira, A. Harju, T. Rabczuk, Amorphized graphene: a stiff material with low thermal conductivity, Carbon, 103 (2016) 318-326.
[27] Z. Fan, W. Chen, V. Vierimaa, A. Harju, Efficient molecular dynamics simulations with many-body potentials on graphics processing units, Computer Physics Communications, 218 (2017) 10-16.
[28] Z. Fan, Z. Zeng, C. Zhang, Y. Wang, K. Song, H. Dong, Y. Chen, T. Ala-Nissila, Neuroevolution machine learning potentials: Combining high accuracy and low cost in atomistic simulations and application to heat

transport, Physical Review B, 104 (2021) 104309.
[29] T. Schaul, T. Glasmachers, J. Schmidhuber, High dimensions and heavy tails for natural evolution strategies, Proceedings of the 13th Annual Conference on Genetic and Evolutionary Computation, (2011) 845-852.
[30] Z. Fan, Improving the accuracy of the neuroevolution machine learning potential for multi-component systems, Journal of Physics: Condensed Matter, 34 (2022) 125902.
[31] Z. Fan, Y. Wang, P. Ying, K. Song, J. Wang, Y. Wang, Z. Zeng, K. Xu, E. Lindgren, J.M. Rahm, GPUMD: A package for constructing accurate machine-learned potentials and performing highly efficient atomistic simulations, The Journal of Chemical Physics, 157 (2022) 114801.
[32] G. Kresse, J. Furthmüller, Efficiency of ab-initio total energy calculations for metals and semiconductors using a plane-wave basis set, Computational Materials Science, 6 (1996) 15-50.
[33] G. Kresse, D. Joubert, From ultrasoft pseudopotentials to the projector augmented-wave method, Physical Review B, 59 (1999) 1758.
[34] V. Wang, N. Xu, J.-C. Liu, G. Tang, W.-T. Geng, VASPKIT: A user-friendly interface facilitating high-throughput computing and analysis using VASP code, Computer Physics Communications, 267 (2021) 108033.
[35] H. Yanxon, D. Zagaceta, B. Tang, D.S. Matteson, Q. Zhu, PyXtal_FF: a python library for automated force field generation, Machine Learning: Science and Technology, 2 (2020) 027001.
[36] X. Yu, R. Li, T. Shiga, L. Feng, M. An, L. Zhang, J. Shiomi, N. Yang, Hybrid thermal transport characteristics of doped organic semiconductor poly (3, 4-ethylenedioxythiophene): tosylate, The Journal of Physical Chemistry C, 123 (2019) 26735-26741.
[37] R. Kubo, M. Toda, N. Hashitsume, Statistical Physics II: Nonequilibrium Statistical Mechanics, Springer Science & Business Media, Berlin, 2012.
[38] H. Meng, X. Yu, H. Feng, Z. Xue, N. Yang, Superior thermal conductivity of poly (ethylene oxide) for solid-state electrolytes: A molecular dynamics study, International Journal of Heat and Mass Transfer, 137 (2019) 1241-1246.
[39] R. Kubo, Statistical-mechanical theory of irreversible processes. I. General theory and simple applications to magnetic and conduction problems, Journal of the Physical Society of Japan, 12 (1957) 570-586.
[40] K. Momma, F. Izumi, VESTA 3 for three-dimensional visualization of crystal, volumetric and morphology data, Journal of Applied Crystallography, 44 (2011) 1272-1276.
[41] W. Sha, X. Dai, S. Chen, B. Yin, F. Guo, Phonon thermal transport in two-dimensional PbTe monolayers via extensive molecular dynamics simulations with a neuroevolution potential, Materials Today Physics, 34 (2023) 101066.
[42] M.S.B. Hoque, Y.R. Koh, J.L. Braun, A. Mamun, Z. Liu, K. Huynh, M.E. Liao, K. Hussain, Z. Cheng, E.R. Hoglund, High in-plane thermal conductivity of aluminum nitride thin films, ACS Nano, 15 (2021) 9588-9599.
[43] G.A. Slack, R.A. Tanzilli, R. Pohl, J. Vandersande, The intrinsic thermal conductivity of AIN, Journal of Physics and Chemistry of Solids, 48 (1987) 641-647.
[44] L. Lindsay, D. Broido, T. Reinecke, Ab initio thermal transport in compound semiconductors, Physical Review B, 87 (2013) 165201.

# Investigating Thermal Transport across the AlN/Diamond Interface via the Machine Learning Potential

Zhanpeng Sun [1, 2, #], Xiang Sun [1, 2, #], Zijun Qi [1, 2], Qijun Wang [1, 2], Rui Li [1, 2], Lijie Li [5], Gai Wu [1, 2, 3, *], Wei Shen [1, 2, 3, *], Sheng Liu [1, 2, 4]

[1] The Institute of Technological Sciences, Wuhan University, Wuhan 430072, China

[2] School of Power and Mechanical Engineering, Wuhan University, Wuhan 430072, China

[3] Hubei Key Laboratory of Electronic Manufacturing and Packaging Integration, Wuhan University, Wuhan 430072, China

[4] School of Mechanical Science and Engineering, Huazhong University of Science and Technology, Wuhan 430074, China

[5] College of Engineering, Swansea University, Swansea SA1 8EN, UK

[*] Corresponding Authors:

Gai Wu, E-mail: wugai1988@whu.edu.cn

Wei Shen, E-mail: wei_shen_@whu.edu.cn

[#] Zhanpeng Sun and Xiang Sun contributed equally to this work.

## ABSTRACT

Aluminum nitride (AlN) is an ultrawide-bandgap semiconductor with excellent potential for high-power applications. However, the heat dissipation issue remains a huge challenge for the use of AlN in high-power devices. A promising solution for this problem is to integrate AlN with the diamond heat sink. Therefore, interfacial thermal transport has become a significant bottleneck in thermal management. In this work, one neuroevolution potential is developed based on neural networks, which significantly improves the accuracy of predicting thermal properties compared to traditional potentials and address the issue of inaccurate thermal performance prediction of AlN/diamond heterostructures using traditional potentials. Molecular dynamics simulations based on NEP is adopted to investigate the crystal-orientation-dependent and interfacial-atom-dependent thermal boundary resistance of the AlN/diamond heterostructures after the interfacial bonding.

Compared to bonding with Al and C atoms, the TBR decreases by approximately 50% after bonding with N and C atoms at the interface. Especially for the AlN (0001)-N-diamond (100) heterostructure, the TBR is 0.95 $m^2 \cdot K \cdot GW^{-1}$, very close to the theoretical limit of 0.8 $m^2 \cdot K \cdot GW^{-1}$ through the diffuse mismatch model (DMM) theory. Finally, the insightful optimization strategies are proposed in this work which could pave the way for better thermal design and management of AlN/diamond heterostructures.

***Keywords:*** Thermal boundary resistance, AlN/diamond interface, Molecular dynamics, Neuroevolution potential

## 1. Introduction

Recently, Aluminum nitride (AlN) has received widespread attention due to its excellent mechanical and electrical properties [1-3]. Due to its outstanding properties such as high breakdown voltage, high electron mobility, stable high-temperature performance and good UV transmittance, AlN has been widely employed in high-power devices in communications, medical, industrial manufacturing and other fields [4]. However, the heat dissipation issue remains a huge challenge for the application of AlN in high-power devices [5]. An excellent solution is the integration of the high thermal conductivity materials with AlN to enhance the heat dissipation [6-9]. Diamond is recognized as a promising candidate for heat sinks due to its high thermal conductivity (over 2000 $W \cdot m^{-1} \cdot K^{-1}$) [10-13]. In addition, the lattice match between AlN and diamond is excellent, and the lower limit of thermal boundary resistance (TBR) for the AlN/diamond interface predicted by the diffuse mismatch model (DMM) theory is 0.8 $m^2 \cdot K \cdot GW^{-1}$ [14]. Therefore, AlN and diamond are widely regarded as promising partners.

Molecular dynamics (MD) simulations have been extensively employed to investigate the interfacial thermal transport properties of heterostructures [15-17]. However, MD simulations rely heavily on the accuracy of the interatomic potential [18]. Heterostructures are typically intricate structures composed of multiple elements, thus making it difficult for traditional potentials to provide an accurate description. This discrepancy may lead to inaccuracies in the evaluation of the TBR of heterostructures using MD methods. For instance, in a prior study, the TBR of AlN/diamond was assessed using MD methods with the Tersoff potential. Despite significant enhancements in interfacial heat transfer achieved through interface engineering, the evaluated TBR still exceeded the theoretical limit by 2 to 3 times [5].

Recent research has utilized machine learning (ML) for studying thermal transport [19-21]. In this method,

the *ab initio* potential energy surface is reconstructed using ML to achieve precise interatomic potential descriptions. Employing ML potential, other researchers have recently explored the thermal properties of graphene/borophene [22], Ge/GaAs [23], GaN/BAs [24] and so on. Compared with other ML algorithms, the neuroevolution potential (NEP) acquired via Graphics Processing Units Molecular Dynamics code (GPUMD) demonstrates superior accuracy and cost-effectiveness in atomistic simulations and heat transport applications [25-28].

In this work, the TBR of the AlN/diamond interfaces was investigated via ML potential. NEP trained specifically for AlN/diamond heterostructures were validated to exhibit improved accuracy compared to traditional potential. Concurrently, the influence of diamond crystal orientations and AlN atomic type at interfaces on TBR was also investigated. Furthermore, a more accurate potential was provided for MD simulations of heat transport in AlN/diamond heterostructures. Guided by the crystal orientations of diamond and the atomic types of AlN at the interface, insightful optimization strategies were proposed, paving the way for better thermal design and management of AlN/diamond heterostructures.

## 2. Computational methods and models

### 2.1 NEP method

The NEP model, a machine learning potential (MLP), utilizes a single neural network and is trained through a separable natural evolution strategy [29]. The NEP model generates the potential energy surface function *Ui* for atom *i* by constructing the descriptor vector $q_v^i$ ,which can be computed using the following formula [28, 30, 31]:

$$U_i = \sum_{\mu=1}^{N_{neu}} \omega_\mu^{(1)} \, tanh\left(\sum_{v=1}^{N_{des}} \omega_{\mu v}^{(0)} q_v^i - b_\mu^{(0)}\right) - b^{(1)} \quad (1)$$

where $N_{des}$ represents the number of components in the descriptor vector, $N_{neu}$ denotes the number of neurons, $tanh(x)$ stands for the activation function of the hidden layer, $\omega^{(0)}$ represents the weight matrix connecting the input layer to the hidden layer, $\omega^{(1)}$ represents the weight vector connecting the hidden layer to the output layer node $U_i$, $b^{(0)}$ is the bias vector of the hidden layer, and $b^{(1)}$ is the bias of the output layer node $U_i$. As illustrated in Fig. 1 (a), the NEP model comprises three layers: input, hidden, and output layers. In this study, the hidden layer consists of 60 neurons.

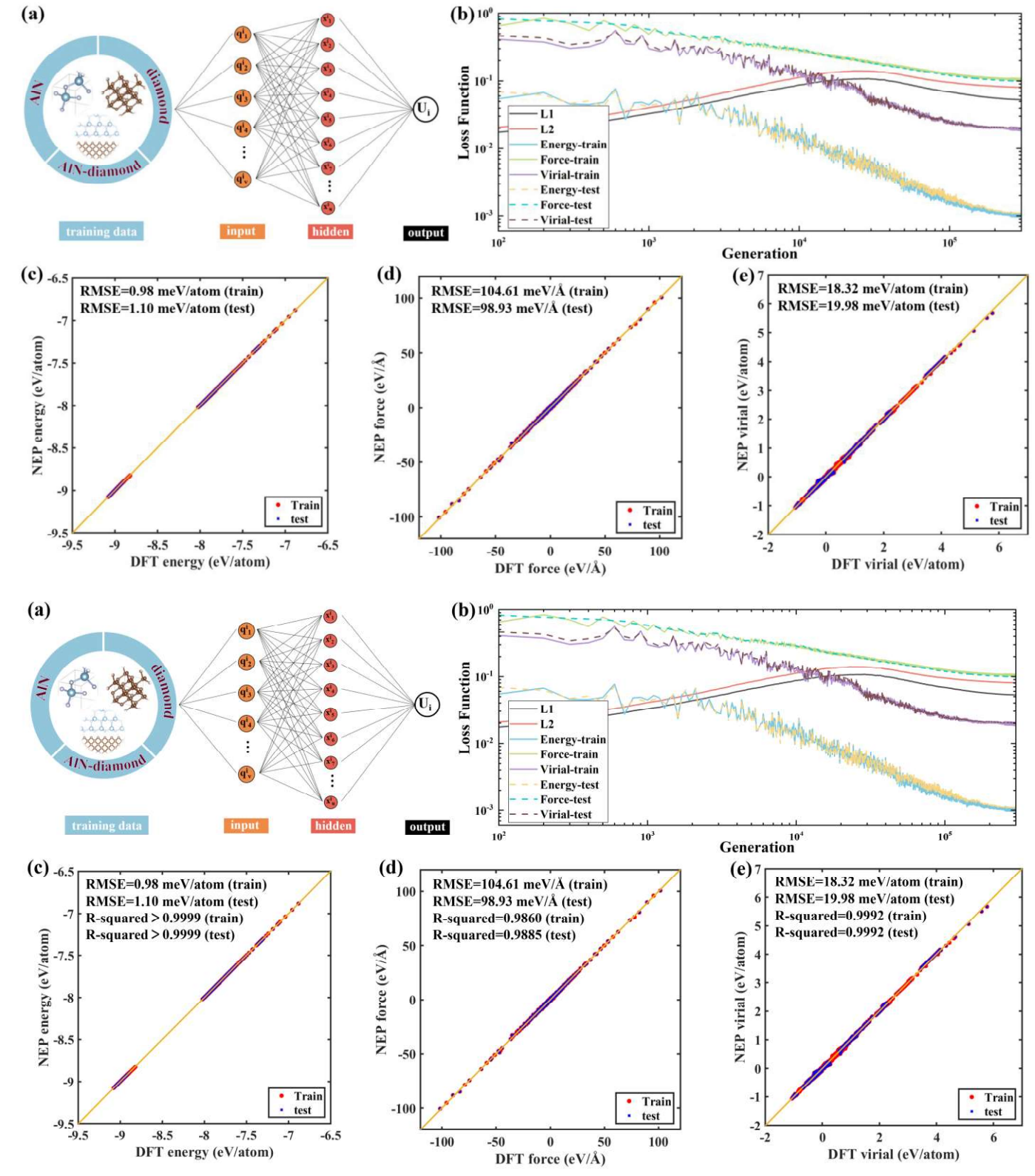


**Fig. 1.** (a) Simplified schematic representation of the NEP framework. (b) Evolution of loss functions during the training process. L1 and L2 are regularizations. (c)–(e) Comparison between the NEP predictions and DFT reference values of energy, force, and virial for the training and test sets.

## 2.2 Details of training data and mechanical behavior

For exploring heat transfer at the AlN/diamond interface, a training dataset has been built, comprising AlN, diamond, and their heterostructures. In order to be more consistent with the situation in the experiment,

primary consideration is given to the (0001) planes of AlN and the (100), (110), and (111) planes of diamond. Simultaneously, the Al-C ~~or~~ and N-C bonding at the interface of AlN/diamond including the reconstructed (100) surface of diamond haves also been ~~also~~ taken into account. Therefore, there are 6 types of heterostructures in the training set. The MD trajectories have been obtained through *ab initio* MD simulations using the Vienna *Ab Initio* Simulation Package (VASP) [32, 33], and the creation of the heterostructures in this work has mainly been conducted based on the VASPKIT [34]. Finally, *ab initio* configurations of 600 pristine AlN, 600 pristine diamond, and 2600 heterostructures have been obtained, among which 2500 configurations are included in the training dataset and 1300 configurations are included in the test dataset.

The loss terms for energy, force, and virial relations in the test and training datasets show very good convergence after 300000 generations as depicted in Fig. 1 (b). Figure 1 (c-e) display parity plots illustrating the correlations between the energies, atomic forces, and atomic virial relations predicted by the NEP and DFT, indicating strong agreement. The root-mean-squared error (RMSE) and R-squared values for the predictions are~~is~~ provided as well. Typically, the RMSE values of each trained MLP model fall in the range of several meV/atom in terms of energy and several hundred meV/Å in terms of force, and all of the R-squared values for the training and test dataset are as high as more than 0.985, both indicating satisfactory training [35]. Table 1 illustrates the training hyperparameters.

**Table 1**. NEP training hyperparameters.

| Parameter | Value | Parameter | Value |
|---|---|---|---|
| $r_C^R$ | 8 Å | $r_C^A$ | 5 Å |
| $n_{max}^R$ | 12 | $n_{max}^A$ | 8 |
| $N_{basis}^R$ | 8 | $N_{basis}^A$ | 8 |
| $l_{max}^{3b}$ | 4 | $l_{max}^{4b}$ | 2 |
| $l_{max}^{5b}$ | 0 | $\lambda_1$ | 0.05 |
| $\lambda_2$ | 0.05 | $\lambda_e$ | 1.0 |
| $\lambda_f$ | 1.0 | $\lambda_v$ | 0.1 |
| $N_{neuron}$ | 60 | $N_{batch}$ | 1050 |
| $N_{population}$ | 50 | $N_{generation}$ | 300000 |

## 2.3 Equilibrium molecular dynamics (EMD) method and models

EMD simulations are employed to evaluate the thermal conductivity, based on the Green-Kubo approach [36-38]. The Green-Kubo formula connects fluctuations in heat current to thermal conductivity through the use of the autocorrelation function, as follows [39]:

$$k_\alpha(t) = \frac{1}{k_B T^2 V} \int_0^{t_0} < J_\alpha(0) J_\alpha(t) > dt \quad (2)$$

where $k_\alpha$ signifies the thermal conductivity in the α direction, $k_B$ denotes the Boltzmann

constant, $V$ represents the volume of the model cell, $T$ stands for the temperature, $t_0$ indicates the integral upper limit, $J_\alpha$ denotes the component of heat current $J$ in the α direction, and $< J_\alpha(0) J_\alpha(t) >$ represents the ensemble average.

AlN has a *P63mc* crystal symmetry, and each conventional unit cell includes 2 aluminum atoms and 2 nitrogen atoms. Diamond has an *Fd-3m* crystal symmetry, and each conventional unit cell contains 8 carbon atoms. In EMD simulation, the bulk of the AlN system, consisting of $16 \times 9\sqrt{3} \times 9$ conventional unit cells, includes 10368 atoms, and the bulk of the diamond system, consisting of $10 \times 10 \times 10$ conventional unit cells, includes 8000 atoms. Convergence tests on the model sizes have been conducted, as shown in Fig. 2. In order to exclude the size effect, the thermal conductivity at different atomic scales at 300 K has been calculated, such as the diamond with 4096, 5832 and 8000 atoms and the AlN with 6656, 8424 and 10368 atoms. It can be found that the differences in thermal conductivities among diamond and AlN structures for different cell sizes are within 5%. Thus, it can be further considered that the size effect of the thermal conductivity calculations for diamond and AlN structures in this work can be ignored. In this work, cell structures have been visualized using VESTA software [40]. Periodic boundary conditions have been applied in all three directions. To reduce calculation errors, 50 independent MD runs have been performed to obtain the average κ values with time steps of 1 fs at 300 K.

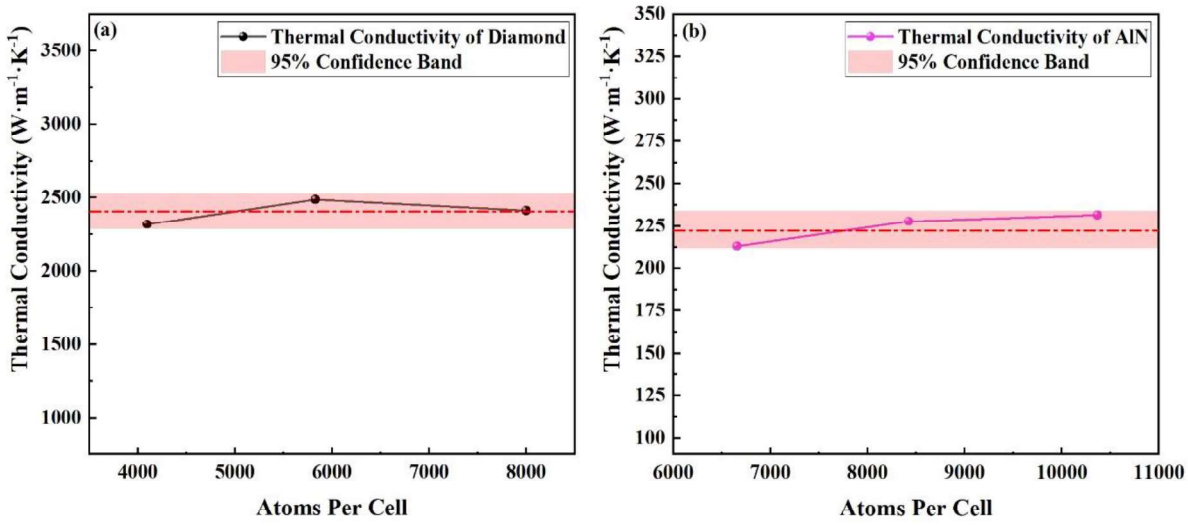


**Fig. 2.** The thermal conductivities of (a) diamond and (b) AlN with the increase of the cell size

## 2.4 Non-equilibrium molecular dynamics (NEMD) method and models

The Non-equilibrium Molecular Dynamics (NEMD) method, based on Fourier's law, divides the system into three distinct regions: a heat source continually supplying energy, a heat sink continuously releasing energy, and a measurement component for evaluating thermal conductivity. Strict adherence to the principle

of energy conservation is essential in NEMD simulations. If the interatomic potential lacks sufficient accuracy, it will be very challenging to maintain a consistent energy flow from the heat source to the heat sink, the system will also collapse during the NEMD simulation [41]. Thus, NEMD simulations serve as a measure of stability for NEP. Fig. 3(b) indicates that the energy values of the heat source entering the system and the heat sink leaving the system are distributed symmetrically around E = 0, satisfying the law of energy conservation. This symmetry also confirms the sufficient accuracy of our NEP. The heat flux $J_Q$ generated in the NEMD process can be defined as:

$$J_Q = \frac{|dQ/dt|}{A} \tag{3}$$

where $|dQ/dt|$ and $A$ signify the energy exchange rate and the area of the simulation box perpendicular to the heat fluent, respectively. In order to mitigate the influence of interface area variation, the interface area of the model is set to a uniform size. The temperature difference ΔT is obtained from the temperature distribution in the abovementioned interface region. The thermal boundary resistance (TBR) can be considered analogous to the thermal conductivity and be calculated as the formula [14]:

$$\mathrm{TBR} = \frac{\Delta \mathrm{T}}{J_Q} \tag{4}$$

A time step of 0.5 fs has been employed. Initially, a 0.1 ns heat bath has been utilized to stabilize the system temperature at 300 K, followed by a 0.5 ns equilibration period to stabilize the heat flow using the Langevin thermostat. Subsequently, the temperature profile has been acquired by running the system for 2 ns. The pertinent data are sampled every 1000 time steps and averaged every 50 data points before recording. This process has been iterated 80 times, and the ultimate temperature profile has been derived through averaging. Considering the real-world industrial scenarios, a heat source ($T_{source}$ = 325 K) and a heat sink ($T_{sink}$ = 275 K) are positioned at the ends of AlN and diamond, respectively. The heat flux proceeds from AlN to diamond. Throughout the simulation, the outermost layers in the *z* direction on both sides have been kept fixed to ensure contact with each other. Periodic boundary conditions have been applied in the *x* and *y* directions. The model size surpasses 5 × 5 × 30 nm³, encompassing over 100000 atoms (with slight variations depending on crystal orientation), as depicted in Fig. 3 (a). In heterogeneous structures composed of different crystal orientations, the mismatch between AlN and diamond in the *x*-*y* plane are all less than 1%.

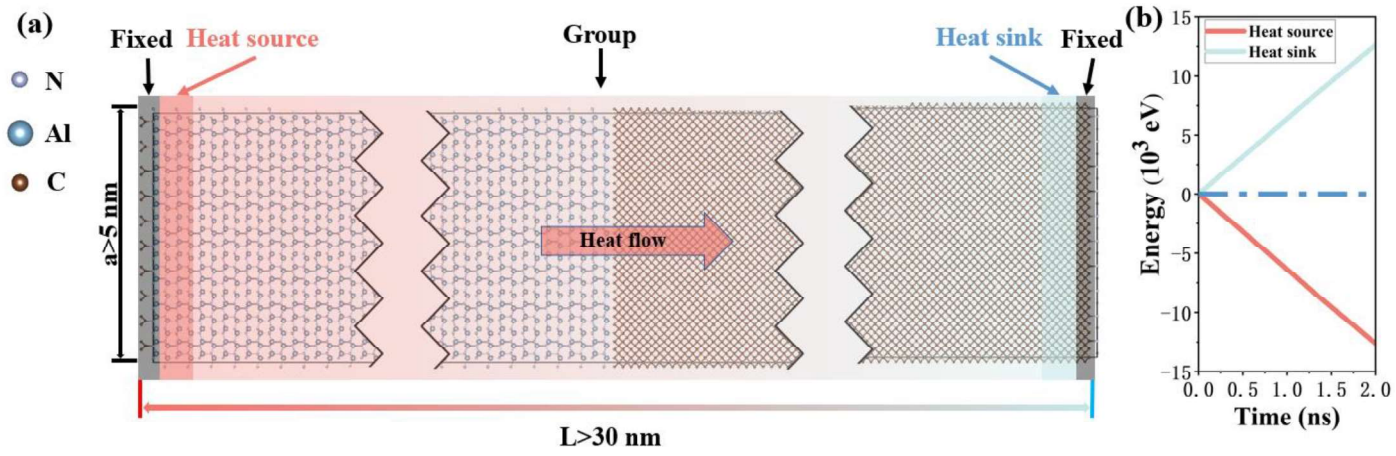


**Fig. 3.** (a) Schematic diagram of NEMD simulation. (b) The cumulative energy of the heat source domain and heat sink domain varying as a function of the simulation time.

# 3. Results and discussion

## 3.1 Bulk thermal properties

Phonon dispersion is regarded as one of the most important thermal properties, which is also commonly used for evaluating the interatomic potentials. As depicted in Fig. 4 (a, b), the phonon dispersion of AlN and diamond calculated by NEP exhibits strong agreement with the results calculated by DFT (density functional theory) method. It is demonstrated that NEP can relatively accurately predict the thermal properties of AlN and diamond. The thermal conductivity values of diamond and AlN predicted by NEP at 300 K are shown in Fig. 4 (c). From Fig. 4 (d, e), it can be observed that while the thermal conductivity values of AlN and diamond predicted by NEP are lower than those predicted by DFT, they both exhibit better performance compared to the predictions by Tersoff. The predicted thermal conductivity based on DFT serves as the standard level, the increase predicted by NEP is 4.33% for AlN and 40.65% for diamond compared to the predictions by Tersoff. Furthermore, the thermal conductivity values predicted by NEP demonstrate excellent agreement with the reported experimental results [11, 42]. In conclusion, the NEP trained through ML will have a better performance than the traditional Tersoff potential in predicting the interfacial heat transfer in AlN/diamond heterostructures.

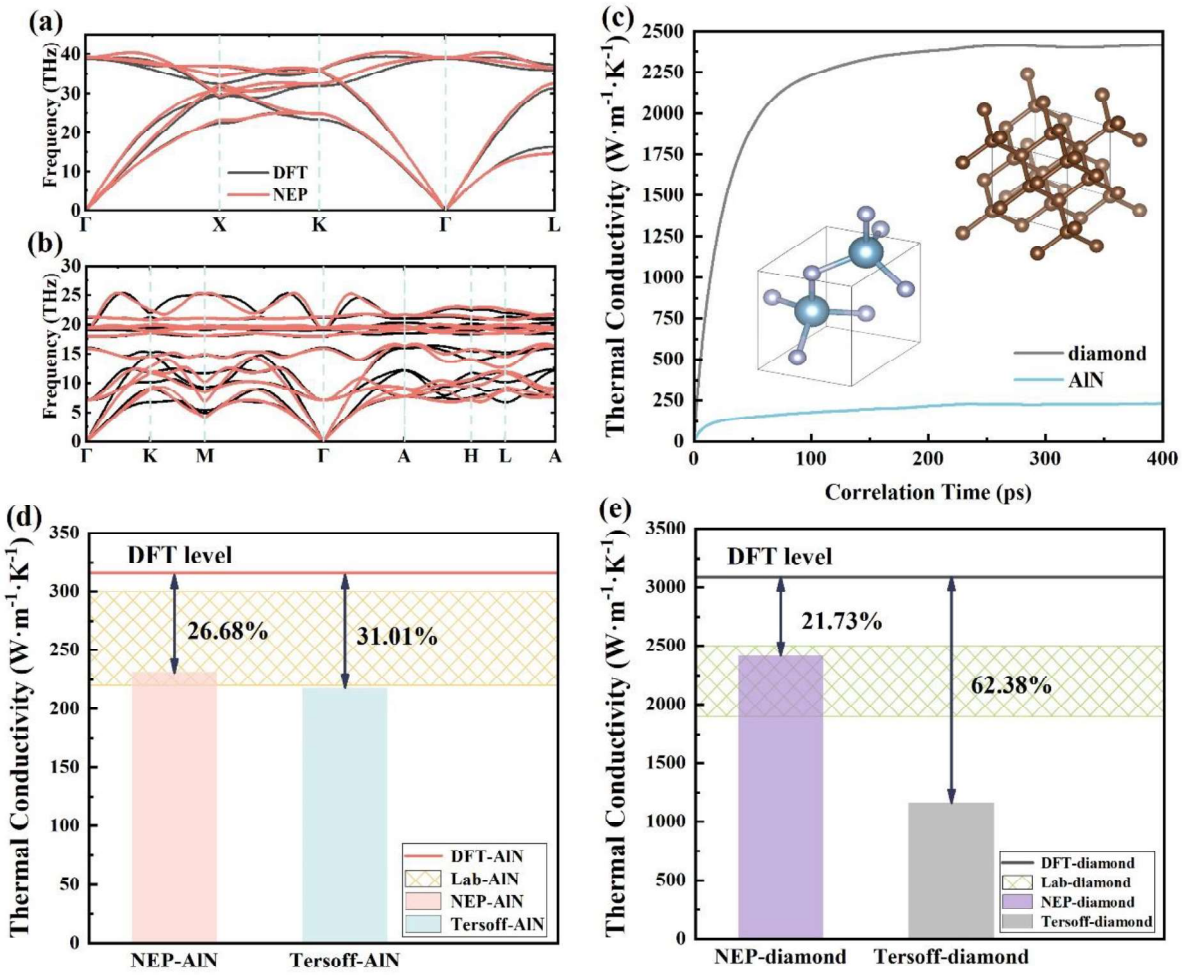


**Fig. 4.** Phonon dispersion of (a) diamond, (b) AlN. (c) Thermal conductivity of diamond and AlN at 300 K as a function of correlation time using the Green–Kubo method with the NEP, each of which is the average of 50 independent simulations. (d) A comparison between the thermal conductivity values of AlN predicted by NEP, Tersoff [5], DFT [43, 44], and experimental measurements [42]. (e) A comparison between the thermal conductivity values of diamond predicted by NEP, Tersoff [5], DFT [12], and experimental measurements [11].

## 3.2 Heat transfer in AlN/diamond interfaces

Further investigation into the interfacial heat transfer in AlN/diamond heterostructures is conducted through NEMD simulations using NEP. The stable temperature distributions of AlN/diamond heterostructures, which consist of various interfaces between AlN and diamond, are displayed in Fig. 5 (a–f). An evident temperature jump (ΔT) is observed at the AlN/diamond interface, implying the presence of a finite TBR between AlN and diamond. The TBR of the AlN (0001)-Al-diamond (100/110/111) heterostructures by interfacial bonding are all approximately 1.8 $m^2 \cdot K \cdot GW^{-1}$. Compared to previous studies using traditional potentials, the TBR increases by approximately 17%, mainly attributed to NEP's more accurate prediction of the thermal properties of AlN and diamond [5]. The TBR of the AlN (0001)-N-diamond (100/110/111) heterostructures by interfacial bonding are all approximately 1.0 $m^2 \cdot K \cdot GW^{-1}$. Especially for the AlN (0001)-N-diamond (100) heterostructure, the TBR is 0.95 $m^2 \cdot K \cdot GW^{-1}$, very close to the theoretical limit of 0.8

$m^2 \cdot K \cdot GW^{-1}$. We can observe that the crystal orientation of diamond has a relatively minor impact on TBR, whereas the bond atom types of AlN at the interface has a significant influence on TBR. The TBR of N-C bonding is nearly 50% lower than that of Al-C bonding. To further explore the reasons behind this phenomenon, the vibrational density of states (VDOS) is calculated, as shown in Fig. 6. The overlap of VDOS between N atoms and C atoms is higher compared to Al atoms and C atoms. In the AlN/diamond heterostructure, heat transfer primarily relies on lattice vibrations. The higher overlap of VDOS between N and C atoms indicates that the vibrational frequencies of N and C atoms are closer, leading to a more effective lattice vibration transmission. It is indicated to be the key reason for the lower TBR of N-C bonding compared to Al-C bonding at the interface in the AlN/diamond heterostructures.

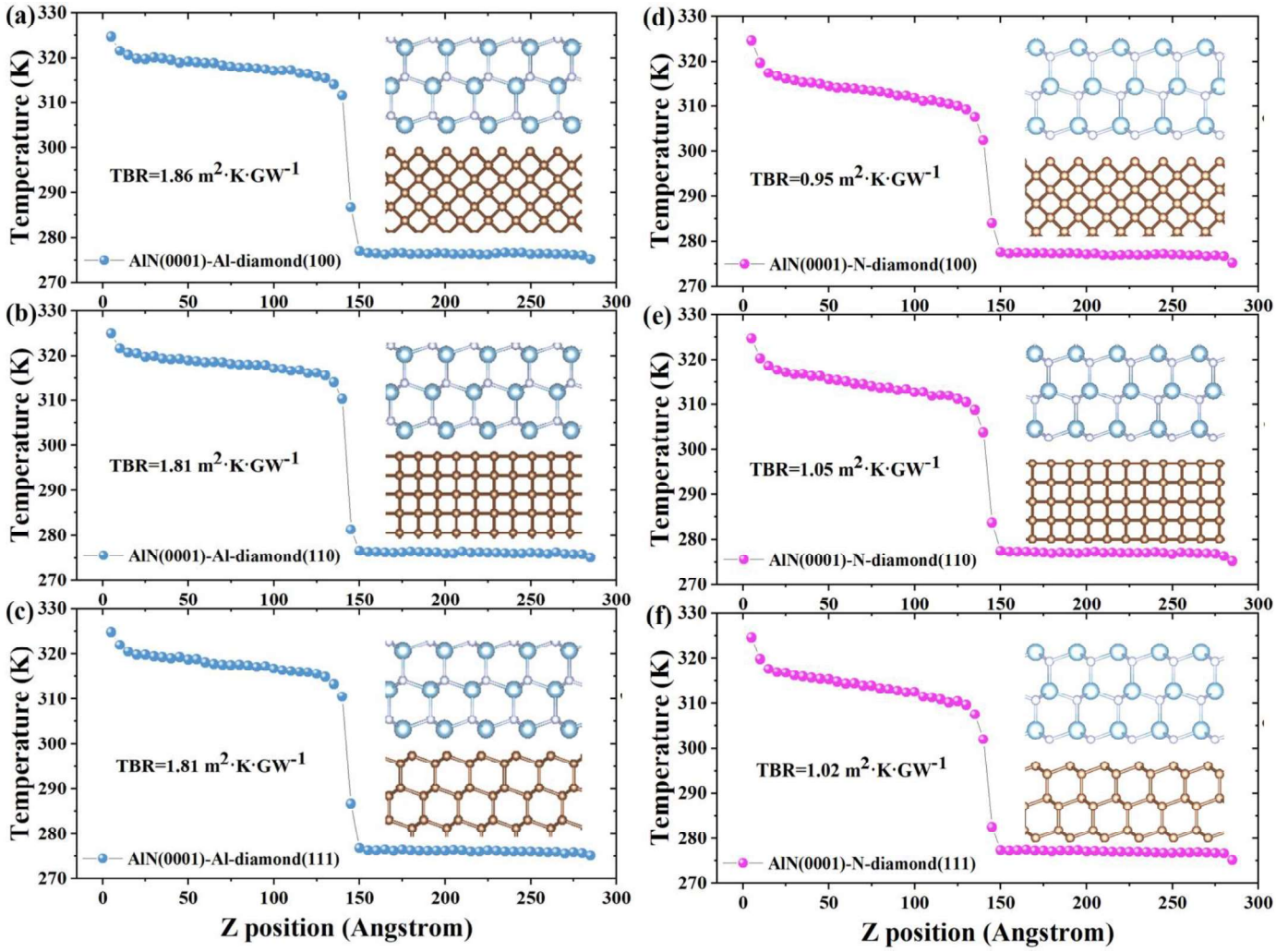

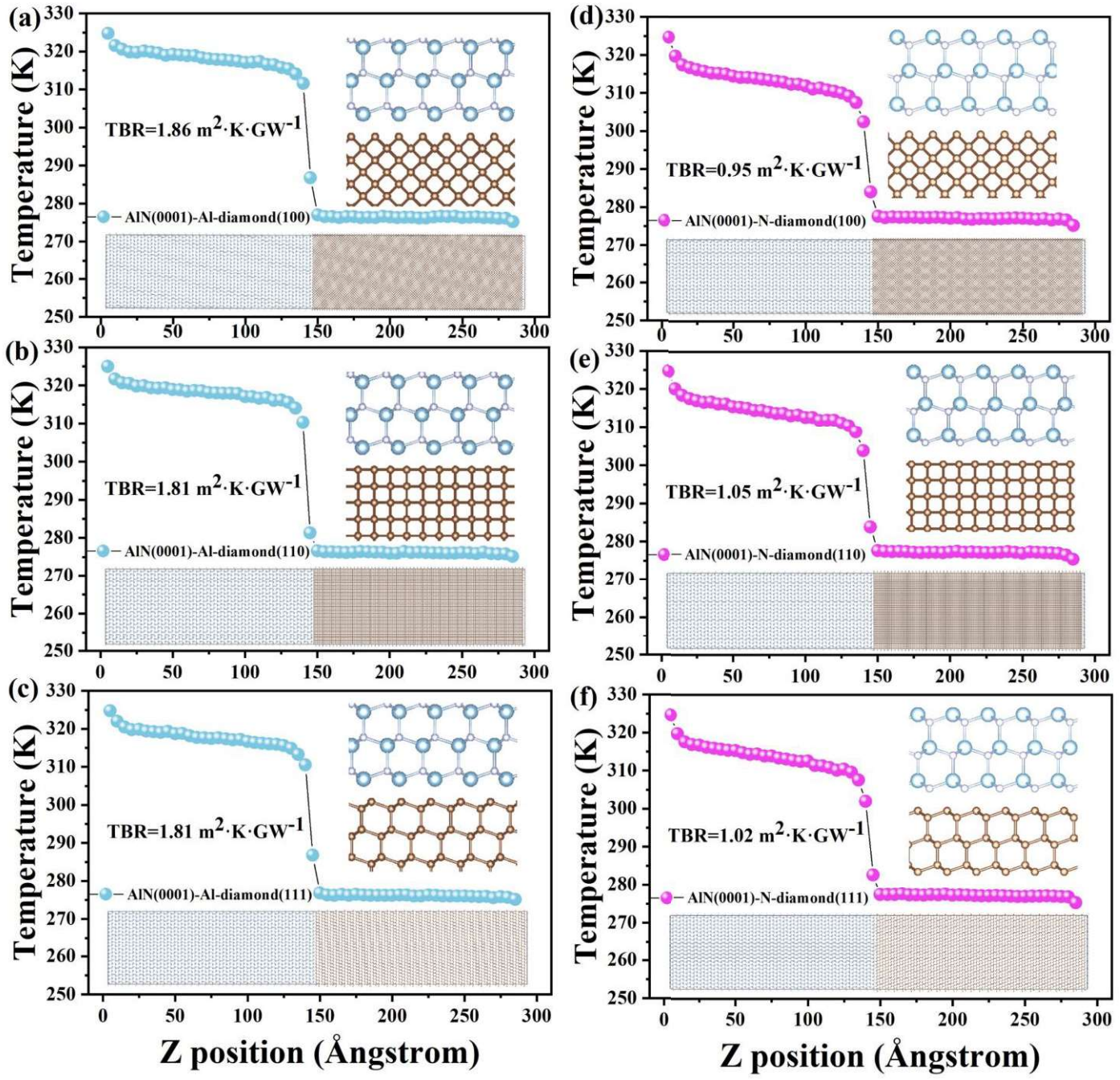


**Fig. 5.** Corresponding temperature profiles of (a) AlN (0001)-Al-diamond (100), (b) AlN (0001)-Al-diamond (110), (c) AlN (0001)-Al-diamond (111), (d) AlN (0001)-N-diamond (100), (e) AlN (0001)-N-diamond (110), and (f) AlN (0001)-N-diamond (111). The bonding at the interface in the figure is in the state before relaxation. Only the structure of the initial state is shown.

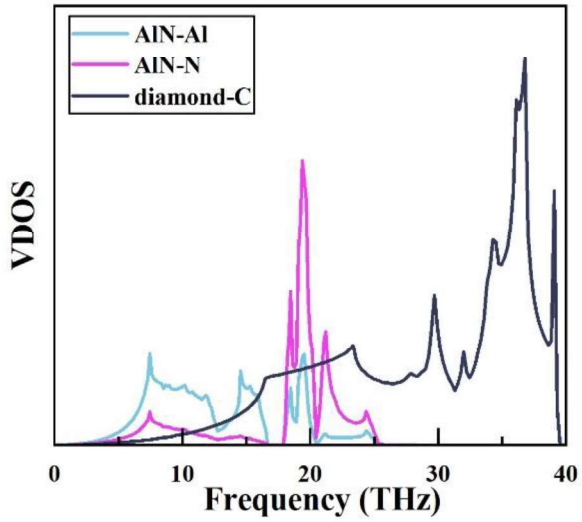


**Fig. 6.** The vibration density of states (VDOS) of AlN-Al/N and diamond-C.

## 4. Conclusion

In summary, an NEP has been trained using GPUMD to predict the thermal transfer properties at the AlN/diamond interface, based on machine learning method. The NEP has been used to predict the phonon dispersions of diamond and AlN, as well as the thermal conductivity at 300 K. The phonon dispersions predicted by NEP are in excellent agreement with the results predicted by DFT. Moreover, the thermal conductivity predicted by NEP at 300 K is in excellent agreement with previously reported experimental measurements. Although the thermal conductivity values predicted by NEP may not reach the level of DFT predictions, there is still a significant improvement compared to traditional potential.

On this basis, the TBR of the six interfaces in the AlN/diamond heterostructures have been predicted. The TBR of the AlN (0001)-Al-diamond (100/110/111) heterostructures by interfacial bonding are all approximately 1.8 $m^2 \cdot K \cdot GW^{-1}$. Compared to previous studies using traditional potentials, the TBR increases by approximately 17%. The TBR of the AlN (0001)-N-diamond (100/110/111) heterostructures by interfacial bonding are all approximately 1.0 $m^2 \cdot K \cdot GW^{-1}$. Especially for the AlN (0001)-N-diamond (100) heterostructure, the TBR is 0.95 $m^2 \cdot K \cdot GW^{-1}$, very close to the theoretical limit of 0.8 $m^2 \cdot K \cdot GW^{-1}$. It can be observed that the crystal orientation of diamond has a minimal effect on TBR, while the atomic types of AlN at the interface has a significant impact on TBR. The TBR of N-C bonding at initial interface is nearly 50% lower than that of Al-C bonding. The VDOS has been calculated to elucidate the mechanism behind this phenomenon. The main reason is that the overlap of VDOS between N and C atoms is higher compared to that between Al and C atoms. Therefore, when the interface is bonded by N atoms and C atoms, heat transfer is more efficient, resulting in a lower TBR.

## Declaration of Competing Interest

The authors declare no conflict of interest.

## Data Availability

The data that support the findings of this study are available from the corresponding author upon reasonable request. The potential file has been uploaded to the GitHub repository and is publicly available at https://github.com/doulala333/NEP-AlN-diamond.

## Acknowledgements

This work was funded by the National Natural Science Foundation of China (Grant Nos. 62004141, 52202045), the Knowledge Innovation Program of Wuhan-Shuguang (Grant Nos. 2023010201020243, 2023010201020255), the Fundamental Research Funds for the Central Universities (Grant Nos. 2042023kf0112, 2042022kf1028), the Major Program (JD) of Hubei Province (Grant No. 2023BAA009), the Hubei Natural Science Foundation (Grant No. 2022CFB606), the Open Fund of Hubei Key Laboratory of Electronic Manufacturing and Packaging Integration (Grant Nos. EMPI2024014, EMPI2024021, EMPI2023027), and the China Scholarship Council (Grant No. 202206275005).

## References

[1] O. Ambacher, Growth and applications of group III-nitrides, Journal of Physics D: Applied Physics, 31 (1998) 2653.
[2] S. Strite, H. Morkoç, GaN, AlN, and InN: a review, Journal of Vacuum Science & Technology B: Microelectronics and Nanometer Structures Processing, Measurement, and Phenomena, 10 (1992) 1237-1266.
[3] J.-M. Zhang, J. Zhang, K.-W. Xu, V. Ji, Structural, electronic and magnetic properties of the Si chains doped zigzag AlN nanoribbons, Physica E: Low-Dimensional Systems and Nanostructures, 65 (2015) 114-119.
[4] R. Yu, G. Liu, G. Wang, C. Chen, M. Xu, H. Zhou, T. Wang, J. Yu, G. Zhao, L. Zhang, Ultrawide-bandgap semiconductor AlN crystals: growth and applications, Journal of Materials Chemistry C, 9 (2021) 1852-1873.
[5] Z. Qi, W. Shen, R. Li, X. Sun, L. Li, Q. Wang, G. Wu, K. Liang, AlN/diamond interface nanoengineering for reducing thermal boundary resistance by molecular dynamics simulations, Applied Surface Science, 615 (2023) 156419.
[6] J.S. Kang, M. Li, H. Wu, H. Nguyen, T. Aoki, Y. Hu, Integration of boron arsenide cooling substrates into gallium nitride devices, Nature Electronics, 4 (2021) 416-423.

[7] Y. Cui, M. Li, Y. Hu, Emerging interface materials for electronics thermal management: experiments, modeling, and new opportunities, Journal of Materials Chemistry C, 8 (2020) 10568-10586.
[8] Y. Cui, Z. Qin, H. Wu, M. Li, Y. Hu, Flexible thermal interface based on self-assembled boron arsenide for high-performance thermal management, Nature Communications, 12 (2021) 1284.
[9] J.S. Kang, H. Wu, Y. Hu, Thermal properties and phonon spectral characterization of synthetic boron phosphide for high thermal conductivity applications, Nano Letters, 17 (2017) 7507-7514.
[10] J. Xiong, Z. Qi, K. Liang, X. Sun, Z. Sun, Q. Wang, L. Chen, G. Wu, W. Shen, Molecular dynamics insights on thermal conductivities of cubic diamond, lonsdaleite and nanotwinned diamond via the machine learned potential, Chinese Physics B, 32 (2023) 680-687.
[11] D. Onn, A. Witek, Y. Qiu, T. Anthony, W. Banholzer, Some aspects of the thermal conductivity of isotopically enriched diamond single crystals, Physical Review Letters, 68 (1992) 2806.
[12] A. Ward, D. Broido, D.A. Stewart, G. Deinzer, Ab initio theory of the lattice thermal conductivity in diamond, Physical Review B, 80 (2009) 125203.
[13] S. Li, Q. Zheng, Y. Lv, X. Liu, X. Wang, P.Y. Huang, D.G. Cahill, B. Lv, High thermal conductivity in cubic boron arsenide crystals, Science, 361 (2018) 579-581.
[14] E.T. Swartz, R.O. Pohl, Thermal boundary resistance, Reviews of Modern Physics, 61 (1989) 605.
[15] K. Ren, X. Liu, S. Chen, Y. Cheng, W. Tang, G. Zhang, Remarkable reduction of interfacial thermal resistance in nanophononic heterostructures, Advanced Functional Materials, 30 (2020) 2004003.
[16] M. Hu, X. Zhang, D. Poulikakos, C.P. Grigoropoulos, Large “near junction” thermal resistance reduction in electronics by interface nanoengineering, International Journal of Heat and Mass Transfer, 54 (2011) 5183-5191.
[17] A. Petkov, A. Mishra, J.W. Pomeroy, M. Kuball, Molecular dynamics study of thermal transport across $Ga_2O_3$–diamond interfaces, Applied Physics Letters, 122 (2023) 031602.
[18] R. Li, Z. Liu, A. Rohskopf, K. Gordiz, A. Henry, E. Lee, T. Luo, A deep neural network interatomic potential for studying thermal conductivity of β-$Ga_2O_3$, Applied Physics Letters, 117 (2020) 152102.
[19] X. Wan, W. Feng, Y. Wang, H. Wang, X. Zhang, C. Deng, N. Yang, Materials discovery and properties prediction in thermal transport via materials informatics: a mini review, Nano Letters, 19 (2019) 3387-3395.
[20] Y.-J. Wu, L. Fang, Y. Xu, Predicting interfacial thermal resistance by machine learning, npj Computational Materials, 5 (2019) 56.
[21] Z. Sun, Z. Qi, K. Liang, X. Sun, Z. Zhang, L. Li, Q. Wang, G. Zhang, G. Wu, W. Shen, A neuroevolution potential for predicting the thermal conductivity of α, β, and ε-$Ga_2O_3$, Applied Physics Letters, 123 (2023) 192202.
[22] B. Mortazavi, E.V. Podryabinkin, S. Roche, T. Rabczuk, X. Zhuang, A.V. Shapeev, Machine-learning interatomic potentials enable first-principles multiscale modeling of lattice thermal conductivity in graphene/borophene heterostructures, Materials Horizons, 7 (2020) 2359-2367.
[23] S. Wyant, A. Rohskopf, A. Henry, Machine learned interatomic potentials for modeling interfacial heat transport in Ge/GaAs, Computational Materials Science, 200 (2021) 110836.
[24] J. Wu, E. Zhou, A. Huang, H. Zhang, M. Hu, G. Qin, Deep-potential enabled multiscale simulation of gallium nitride devices on boron arsenide cooling substrates, Nature Communications, 15 (2024) 2540.
[25] Z. Fan, T. Siro, A. Harju, Accelerated molecular dynamics force evaluation on graphics processing units for thermal conductivity calculations, Computer Physics Communications, 184 (2013) 1414-1425.
[26] B. Mortazavi, Z. Fan, L.F.C. Pereira, A. Harju, T. Rabczuk, Amorphized graphene: a stiff material with low thermal conductivity, Carbon, 103 (2016) 318-326.
[27] Z. Fan, W. Chen, V. Vierimaa, A. Harju, Efficient molecular dynamics simulations with many-body potentials on graphics processing units, Computer Physics Communications, 218 (2017) 10-16.
[28] Z. Fan, Z. Zeng, C. Zhang, Y. Wang, K. Song, H. Dong, Y. Chen, T. Ala-Nissila, Neuroevolution machine learning potentials: Combining high accuracy and low cost in atomistic simulations and application to heat

transport, Physical Review B, 104 (2021) 104309.
[29] T. Schaul, T. Glasmachers, J. Schmidhuber, High dimensions and heavy tails for natural evolution strategies, Proceedings of the 13th Annual Conference on Genetic and Evolutionary Computation, (2011) 845-852.
[30] Z. Fan, Improving the accuracy of the neuroevolution machine learning potential for multi-component systems, Journal of Physics: Condensed Matter, 34 (2022) 125902.
[31] Z. Fan, Y. Wang, P. Ying, K. Song, J. Wang, Y. Wang, Z. Zeng, K. Xu, E. Lindgren, J.M. Rahm, GPUMD: A package for constructing accurate machine-learned potentials and performing highly efficient atomistic simulations, The Journal of Chemical Physics, 157 (2022) 114801.
[32] G. Kresse, J. Furthmüller, Efficiency of ab-initio total energy calculations for metals and semiconductors using a plane-wave basis set, Computational Materials Science, 6 (1996) 15-50.
[33] G. Kresse, D. Joubert, From ultrasoft pseudopotentials to the projector augmented-wave method, Physical Review B, 59 (1999) 1758.
[34] V. Wang, N. Xu, J.-C. Liu, G. Tang, W.-T. Geng, VASPKIT: A user-friendly interface facilitating high-throughput computing and analysis using VASP code, Computer Physics Communications, 267 (2021) 108033.
[35] H. Yanxon, D. Zagaceta, B. Tang, D.S. Matteson, Q. Zhu, PyXtal_FF: a python library for automated force field generation, Machine Learning: Science and Technology, 2 (2020) 027001.
[36] X. Yu, R. Li, T. Shiga, L. Feng, M. An, L. Zhang, J. Shiomi, N. Yang, Hybrid thermal transport characteristics of doped organic semiconductor poly (3, 4-ethylenedioxythiophene): tosylate, The Journal of Physical Chemistry C, 123 (2019) 26735-26741.
[37] R. Kubo, M. Toda, N. Hashitsume, Statistical Physics II: Nonequilibrium Statistical Mechanics, Springer Science & Business Media, Berlin, 2012.
[38] H. Meng, X. Yu, H. Feng, Z. Xue, N. Yang, Superior thermal conductivity of poly (ethylene oxide) for solid-state electrolytes: A molecular dynamics study, International Journal of Heat and Mass Transfer, 137 (2019) 1241-1246.
[39] R. Kubo, Statistical-mechanical theory of irreversible processes. I. General theory and simple applications to magnetic and conduction problems, Journal of the Physical Society of Japan, 12 (1957) 570-586.
[40] K. Momma, F. Izumi, VESTA 3 for three-dimensional visualization of crystal, volumetric and morphology data, Journal of Applied Crystallography, 44 (2011) 1272-1276.
[41] W. Sha, X. Dai, S. Chen, B. Yin, F. Guo, Phonon thermal transport in two-dimensional PbTe monolayers via extensive molecular dynamics simulations with a neuroevolution potential, Materials Today Physics, 34 (2023) 101066.
[42] M.S.B. Hoque, Y.R. Koh, J.L. Braun, A. Mamun, Z. Liu, K. Huynh, M.E. Liao, K. Hussain, Z. Cheng, E.R. Hoglund, High in-plane thermal conductivity of aluminum nitride thin films, ACS Nano, 15 (2021) 9588-9599.
[43] G.A. Slack, R.A. Tanzilli, R. Pohl, J. Vandersande, The intrinsic thermal conductivity of AIN, Journal of Physics and Chemistry of Solids, 48 (1987) 641-647.
[44] L. Lindsay, D. Broido, T. Reinecke, Ab initio thermal transport in compound semiconductors, Physical Review B, 87 (2013) 165201.
.